



Cite this: *Chem. Sci.*, 2018, **9**, 8723

All publication charges for this article have been paid for by the Royal Society of Chemistry

Received 15th July 2018  
Accepted 16th September 2018

DOI: 10.1039/c8sc03132k

[rsc.li/chemical-science](http://rsc.li/chemical-science)

# Stibine-protected $\text{Au}_{13}$ nanoclusters: syntheses, properties and facile conversion to GSH-protected $\text{Au}_{25}$ nanocluster<sup>†</sup>

Ying-Zhou Li, Rakesh Ganguly, Kar Yiu Hong, Yongxin Li, Malcolm Eugene Tessensohn, Richard Webster and Weng Kee Leong \*

Monostibine-protected ionic  $\text{Au}_{13}$  nanoclusters, namely,  $[\text{Au}_{13}(\text{L})_8(\text{Cl})_4][\text{Cl}]$  ( $\text{L} = \text{SbPh}_3$ , **2a**·Cl;  $\text{Sb}(\text{p-tolyl})_3$ , **2b**·Cl) were prepared by the direct reduction of  $\text{Au}(\text{L})\text{Cl}$  with  $\text{NaBH}_4$  in dichloromethane. Anion exchange with **2a**·Cl afforded  $[\text{Au}_{13}(\text{SbPh}_3)_8(\text{Cl})_4][\text{X}]$  ( $\text{X} = \text{PF}_6^-$ , **2a**· $\text{PF}_6^-$ ;  $\text{BPh}_4^-$ , **2a**· $\text{BPh}_4^-$ ). All these have been characterized by multinuclear NMR, ESI-MS and UV-Vis spectroscopy. Crystallographic analysis of **2a**· $\text{BPh}_4^-$  reveals that the cation possesses  $C_{2v}$  symmetry and the trideca gold core adopts a closed icosahedron configuration. The weaker coordinating ability of the stibine ligands leads to the ready reaction of **2b**·Cl with  $\text{PPh}_3$  or glutathione (GSH) to form the smaller phosphine-protected cluster  $[\text{Au}_{11}(\text{PPh}_3)_8\text{Cl}_2][\text{Cl}]$  or larger thiolate-protected cluster  $\text{Au}_{25}(\text{SG})_{18}$ , respectively. In the latter reaction, the addition of a small amount (0.5 to 3.5 equivalents) of a suitable oxidant such as  $\text{K}_3(\text{Fe}(\text{CN})_6)$  accelerates the conversion rate significantly.

## Introduction

The past decade has witnessed an explosion in the research output on thiolate,<sup>1</sup> and alkynyl-protected<sup>2</sup> gold nanoclusters. The earliest work on what is now generally referred to as Au nanoclusters can, however, be traced back to the pioneering work of Malatesta on phosphine-protected species.<sup>3</sup> A large number of these, with a variety of metal core configurations, have already been structurally characterized. They include some cationic<sup>4</sup> and neutral species<sup>5</sup> with 8–39 gold atoms, as well as some even larger ones for which their sizes have only been estimated, such as,  $[\text{Au}_{55}(\text{PPh}_3)_{12}\text{Cl}_6]$ ,<sup>6</sup> and  $[\text{Au}_{101}(\text{PPh}_3)_{21}(\text{Cl})_5]$ .<sup>7</sup> Among these, the icosahedral  $\text{Au}_{13}$  clusters are of special interest as their cluster core represents an important sub-unit in some of the larger clusters, such as, the homometallic  $\text{Au}_{25}$ ,  $\text{Au}_{37}$ ,  $\text{Au}_{38}$ ,  $\text{Au}_{39}$  and  $\text{Au}_{60}$  clusters,<sup>1b-d,4i,8</sup> and the heterometallic  $\text{Au}_{13}\text{Cu}_n$  ( $n = 2, 4, 8, 12$ ) clusters.<sup>9</sup>

Although the  $\text{Au}_{13}$  cluster core is expected to be thermodynamically stable due to its closed-shell geometry,<sup>10</sup> the synthesis of monodispersed  $\text{Au}_{13}$  clusters remains a challenge. Most of

the studies have been on those protected by diphosphines as they exhibit higher thermodynamic stability arising from the chelating effect of the diphosphine.<sup>4d</sup> The first diphosphine-protected cluster, with the probable formulation  $[\text{Au}_{13}(\text{dppm})_6][\text{NO}_3]_4$ , was prepared by  $\text{NaBH}_4$  reduction of the Au(i) complex  $[\text{Au}_2(\text{dppm})][\text{NO}_3]_2$  (dppm = 1,1-bis(diphenylphosphino)methane) in ethanol.<sup>11</sup> Two other structurally related examples, *viz.*,  $[\text{Au}_{13}(\text{dppm})_6][\text{BPh}_4]_3$  and  $[\text{Au}_{13}(\text{dppm})_6][\text{Cl}]_5$ , which contain open icosahedral metal cores, have also been reported recently; the former was obtained from a dppm-protected  $\text{Au}_{18}$  cluster by thiol-induced size focusing, while the latter resulted from the direct reduction of  $[\text{Au}_2(\text{dppm})(\text{Cl})_2]$  with  $\text{NaBH}_4$  in a solution of methanol and dichloromethane (DCM).<sup>12,13</sup> Interestingly, these three cationic  $\text{Au}_{13}$  clusters have the same composition but carry different charges. A facile two-step approach to diphosphine-protected  $\text{Au}_{13}$  clusters has also been reported; the addition of aqueous HCl to a polydispersed mixture of  $\text{Au}_n$  clusters ( $n = 9–15$ ), obtained from reduction of the corresponding diphosphine-Au(i) complex, was found to induce nuclearity convergence to  $\text{Au}_{13}$  clusters. This method yielded the diphosphine-protected  $\text{Au}_{13}$  clusters  $[\text{Au}_{13}(\text{L}^2)_5(\text{Cl})_2][\text{PF}_6]_3$  and  $[\text{Au}_{13}(\text{L})_4(\text{Cl})_4][\text{Cl}]$  ( $\text{L} = \text{L}^3$ ,  $\text{L}^4$ ,  $\text{L}^5$ ), where  $\text{L}^m$  denotes an alkyl-bridged diphosphine ( $\text{Ph}_2\text{P}(\text{CH}_2)_m\text{PPh}_2$ ).<sup>14</sup> The method failed, however, for monophosphines, and for diphosphines with a longer ( $\text{L}^6$ ) or shorter ( $\text{L}^1$ ) alkyl bridge.

In comparison,  $\text{Au}_{13}$  clusters stabilized by monophosphines are much less well-characterised. Reduction of  $[\text{Au}(\text{L})\text{X}]$  ( $\text{L}$  = monophosphine,  $\text{X}$  = halides,  $\text{SCN}$  or  $\text{NO}_3$ ) with  $\text{NaBH}_4$  gave mainly  $\text{Au}_{11}$  or other smaller clusters,<sup>4a-d,5a,b,15</sup> although minor amounts of  $\text{Au}_{13}$  clusters may also be formed in particular cases

Division of Chemistry & Biological Chemistry, Nanyang Technological University, 21 Nanyang Link, Singapore, 637371. E-mail: [chmlwk@ntu.edu.sg](mailto:chmlwk@ntu.edu.sg)

† Electronic supplementary information (ESI) available: Experimental, crystallographic and computational details; table of crystal and refinement data for **1a**, **1b**, **2a**· $\text{BPh}_4^-$ , **3a** and **3b**; ORTEP and stacking diagrams of **1a**, **1b**, **3a** and **3b**; NMR, ESI-MS and UV-Vis spectra of products and some monitoring reactions; TD-DFT excitation transition data of **2a**; CV spectra of **2a**· $\text{PF}_6^-$ ; percent buried volumes of stibine ligands; optimized coordinates of **1a-c** and **2a**. CCDC (CCDC 1852139–1852143). For ESI and crystallographic data in CIF or other electronic format see DOI: 10.1039/c8sc03132k

(*vide infra*). To our knowledge, only three monophosphine-protected icosahedral  $\text{Au}_{13}$  clusters have been reported. The first was  $[\text{Au}_{13}(\text{PPh}_2\text{Me})_{10}\text{Cl}_2][\text{PF}_6]_3$ , obtained from reaction of the initially formed  $[\text{Au}_{11}(\text{PPh}_2\text{Me})_{10}][\text{PF}_6]_3$  with  $[\text{Et}_4\text{N}]\text{Cl}$  in alcohol.<sup>4f</sup> This was followed 15 years later by  $[\text{Au}_{13}(\text{PPh}_2\text{Me})_8\text{Cl}_4][\text{C}_2\text{B}_9\text{H}_{12}]$ , which was obtained from the reaction of  $[\text{Au}_{11}(\text{PPh}_2\text{Me})_{10}][\text{C}_2\text{B}_9\text{H}_{12}]_3$  with  $[\text{Au}(\text{PPh}_2\text{Me})\text{Cl}]$ .<sup>16</sup> The third example,  $[\text{Au}_{13}(\text{TOP})_8\text{Cl}_4][\text{Cl}]$  (where TOP = trioctylphosphine), was obtained as a minor product from the  $\text{NaBH}_4$  reduction of  $[\text{Au}(\text{TOP})\text{Cl}]$  in aqueous THF.<sup>14b</sup> Of these three examples, only the first (with a P : Cl ratio of 10 : 2) has been fully characterized, while the other two (with P : Cl ratios of 8 : 4) have only been characterized spectroscopically and the exact ligand arrangements have not been unambiguously determined.

In comparison, no stibine-protected Au nanoclusters are known. We present here the first study on monostibine-protected  $\text{Au}_{13}$  nanoclusters with Sb : Cl ratios of 8 : 4, *viz.*,  $[\text{Au}_{13}(\text{L})_8\text{Cl}_4][\text{X}]$  (where L =  $\text{Ph}_3\text{Sb}$ ,  $(p\text{-tolyl})_3\text{Sb}$ ; X = Cl,  $\text{PF}_6$ ,  $\text{BPh}_4$ ), and their conversion to the larger glutathione-stabilised nanocluster  $\text{Au}_{25}(\text{SG})_{18}$ .

## Results and discussion

### Syntheses and characterization

The  $\text{Au}(\text{i})$  stibine complexes  $[\text{Au}(\text{L})\text{Cl}]$  (L =  $\text{SbPh}_3$ , **1a**;  $\text{Sb}(p\text{-tolyl})_3$ , **1b**) could be prepared by the slow addition of an equimolar amount of the stibine into a DCM solution of  $\text{Me}_2\text{SAuCl}$  at room temperature (*ca.* 21 °C) and in the dark. The products were obtained as white solids after removal of the solvent but quickly decomposed on exposure to light, and especially in solution. Crystallographic analyses show that while **1a** is a monomer, the *p*-tolyl analogue **1b** is a dimer with a strong  $\text{Au} \dots \text{Au}$  interaction (Fig. S1–S3†). This difference in structure is probably the result of polymorphism, as both stacking modes have been observed previously in the phosphine analogue  $[(p\text{-tolyl})_3\text{PAuCl}]$ .<sup>17</sup> An ORTEP plot depicting one of the two crystallographically distinct dimeric units observed for **1b** is shown in Fig. 1. The  $\text{Au} \dots \text{Au}$  distance (2.9441(14) Å and 2.9784(16) Å) is typical for the  $\text{Au} \dots \text{Au}$  interaction but is much shorter than that found in its phosphine analogue (3.375 Å). This aurophilic interaction is believed to bear significant influence on the reduction process for the preparation of Au nanoclusters.<sup>18</sup>

The reduction of **1a** and **1b** with 0.25 equivalents of  $\text{NaBH}_4$  in the presence of the free stibine gave the corresponding ionic nanoclusters  $[\text{Au}_{13}(\text{L})_8(\text{Cl})_4][\text{Cl}]$  (L =  $\text{SbPh}_3$ , **2a**·Cl;  $\text{Sb}(p\text{-tolyl})_3$ , **2b**·Cl) (Scheme 1). Unlike the phosphine-protected  $\text{Au}_{11}$  nanoclusters  $[\text{Au}_{11}(\text{PPh}_3)_8\text{Cl}_2][\text{Cl}]$ , these stibine-protected nanoclusters could not be purified by column chromatography but they could be obtained in good purity by precipitation with hexane followed by washing with suitable solvents. Although the isolated yields were relatively low (15% and 30% for **2a**·Cl and **2b**·Cl, respectively), the MS and UV-Vis spectra of the crude products did not show any detectable amounts of nanoclusters of other sizes such as  $\text{Au}_{11}$  (Fig. S30 and S37†). Indeed, fractional crystallization of the crude from DCM/hexane (8/4, v/v) in the dark gave mainly **2**·Cl and a colorless crystalline side product identified as the mononuclear  $\text{Au}(\text{i})$  complexes

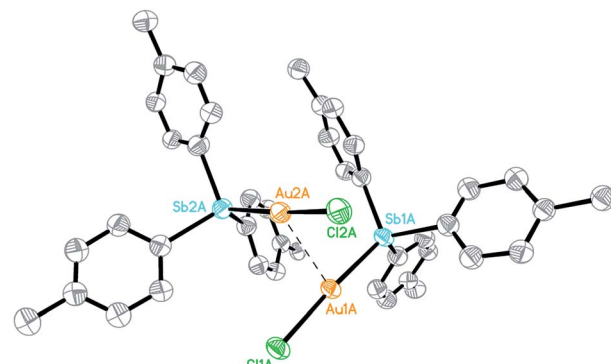
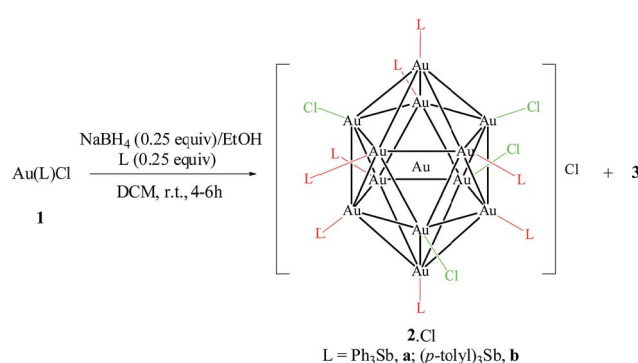


Fig. 1 ORTEP plot depicting one of the two crystallographically distinct dimers of **1b**. Thermal ellipsoids are drawn at the 50% probability level. Organic hydrogen atoms are omitted for clarity. Selected bond lengths (Å):  $\text{Sb}(1\text{A})\text{--Au}(1\text{A}) = 2.460(2)$ ,  $\text{Sb}(2\text{A})\text{--Au}(2\text{A}) = 2.507(2)$ ,  $\text{Au}(1\text{A})\text{--Cl}(1\text{A}) = 2.327(7)$ ,  $\text{Au}(2\text{A})\text{--Cl}(2\text{A}) = 2.259(7)$ ,  $\text{Au}(2\text{A})\text{--Au}(2\text{A}) = 2.9441(14)$ .

$[\text{Au}(\text{SbPh}_3)_4][\text{SbPh}_2\text{Cl}_2]$ , **3a**,<sup>19</sup> and  $[(p\text{-tolyl})_2\text{Cl}_2\text{Sb}]\text{Au}[\text{Sb}(p\text{-tolyl})_3]_3$ , **3b**, respectively. Both **3a** and **3b** were characterized spectroscopically and crystallographically (Fig. S4, S5, S26–S28, S34 and S35†).

The reduction of **1** exhibited markedly different behavior from that of the phosphine analogue  $[\text{Au}(\text{PPh}_3)\text{Cl}]$ . The latter was reported to give the ionic nanocluster  $[\text{Au}_{11}(\text{PPh}_3)_8\text{Cl}_2][\text{Cl}]$  with 0.25 equivalent of  $\text{NaBH}_4$  in DCM but the relatively less stable, neutral nanocluster  $[\text{Au}_{11}(\text{PPh}_3)_7\text{Cl}_3]$  with 5 equivalents of  $\text{NaBH}_4$  in THF.<sup>15</sup> For **1**, reduction with more than 0.25 equivalent of  $\text{NaBH}_4$  led to a decrease in yield without any new nanocluster isolated or observed (Fig. S38†). The use of 5 equivalents of  $\text{NaBH}_4$  (with either DCM or THF as the solvent) led to the immediate formation of an insoluble black precipitate and a colorless supernatant, indicating full decomposition into bulk Au particles. This indicates that while  $\text{NaBH}_4$  can reduce **1** to form **2**·Cl, it also leads to the destruction of **2**·Cl; presumably, the weakly coordinating stibine allows for more ready decomposition and/or aggregation of the gold cores. Addition of a small amount (0.25 equiv.) of the stibine prior to reduction was found to aid the formation of **2**·Cl, but larger amounts (1.0 to 3.0 equiv.) led to lower yields. This is probably related to favoring the formation and/or enhancing the stability of



Scheme 1 Reduction of **1** with  $\text{NaBH}_4$ .



intermediate species, and is consistent with a recent report that the reduction of  $[\text{Au}(\text{PPh}_3)\text{Cl}]$  and  $[\text{Au}(\text{PPh}_3)_2\text{Cl}]$  gave different products.<sup>20</sup> We have similarly observed that reduction of the tetra-stibine coordinated **3a** under the same reaction conditions led to a more complicated mixture, as revealed by the UV-Vis spectrum of the crude mixture, and much less **2a**·Cl was obtained (Fig. S39†). It is also known that steric bulk of the ligand can have a significant influence on the course of the reaction;<sup>21</sup> we tested this with  $\text{SbMes}_3$  (Mes = mesityl), which has a larger percent buried volume (40% for  $\text{SbMes}_3$  vs. 28% for  $\text{SbPh}_3$  and  $\text{Sb}(p\text{-tolyl})_3$ ).<sup>22</sup> The reduction of  $[\text{Au}(\text{SbMes}_3)\text{Cl}]$  (**1c**) under similar reaction conditions, however, afforded a black precipitate in a colorless supernatant; the  $^1\text{H}$  NMR spectrum of the latter showed only  $\text{SbMes}_3$  (Fig. S11†). Presumably, the larger steric bulk of  $\text{SbMes}_3$  prevented nucleation of the intermediate to form nanoclusters.<sup>23</sup>

The chloride anion in **2a**·Cl could be exchanged with  $[\text{PF}_6]^-$  or  $[\text{BPh}_4]^-$  to give **2a**· $\text{PF}_6$  or **2a**· $\text{BPh}_4$ , respectively, as verified by their multinuclear NMR spectra (Fig. S12–S21†). Irrespective of the anion, the  $^1\text{H}$  NMR spectrum is invariant and exhibits three doublets, in an integration ratio of 1 : 2 : 1, in the 7.15–7.50 ppm region (Fig. 2). These resonances are assignable to the *ortho*-H's of the  $\text{SbPh}_3$  ligand, and suggest the presence of three chemically non-equivalent stibine ligand environments. The spectrum of **2b**·Cl similarly exhibits three singlets in a 1 : 2 : 1 integration ratio, in the 2.04–2.11 ppm region, which are ascribable to the methyl protons in three chemically non-equivalent  $\text{Sb}(p\text{-tolyl})_3$  ligand environments (Fig. S20†). This is in contrast to the phosphine-protected nanoclusters  $[\text{Au}_{11}(\text{PPh}_3)_7\text{Cl}_3]$  and  $[\text{Au}_{11}(\text{PPh}_3)_8\text{Cl}_2]\text{Cl}$ , which were reported to show only one set of resonances in their  $^1\text{H}$  and  $^{31}\text{P}$  NMR spectra even down to  $-80^\circ\text{C}$ . Presumably, therefore, the metal cores of **2** are structurally more rigid than the undecagold core in those phosphine-protected nanoclusters.<sup>5a,15</sup>

Crystallographic analysis of a dark red, diffraction-quality crystal of  $2a \cdot BPh_4$  confirmed its chemical formulation, although the crystal exhibited disorder; seven of the peripheral Au atoms were modelled with  $\sim 90 : 10$  disorder. The thirteen gold atoms of the cluster cation are in an icosahedral arrangement, with eight  $SbPh_3$  and four chlorides forming the ligand

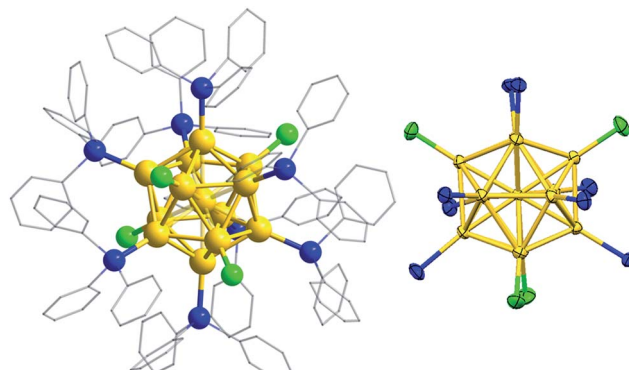


**Fig. 3** Views of the crystal structure of the cationic fragment of **2a**·BPh<sub>4</sub> (left: full structure with hydrogen atoms omitted; right: structure of the core showing the *mm*2 point symmetry). Au: yellow, Sb: blue, Cl: green, C: grey.

sphere (Fig. 3). The presence of one  $\text{BPh}_4^-$  counterion confirmed that the nanocluster is monocationic and consistent with a valence electron count of 8 in accordance with the superatom rule.<sup>24</sup> The electronic structure of **2a**, calculated at the MPW1PW91/LANL2DZ level of theory, clearly shows frontier orbitals corresponding to this superatom complex (Fig. S6†). In fact, the three “HOMO” orbitals may be regarded as comprising a single HOMO ( $-0.258$  eV) and a pair of near-degenerate HOMO – 1 ( $-0.265$  eV), with p orbital characteristics. This is consistent with a breakdown of the icosahedrdal symmetry of the gold core by the ligand sphere; the nanocluster exhibits non-crystallographic  $mm2$  point symmetry. The four Cl ligands lie in two mutually perpendicular planes, dividing the eight  $\text{SbPh}_3$  ligands into three groups in a 1 : 2 : 1 ratio, in agreement with the  $^1\text{H}$  NMR spectrum. The peripheral Au–Au bond lengths (2.8487(10)–2.9248(11) Å) are clearly longer than those from the central Au atom (2.7151(10)–2.7629(10) Å), and comparable to those in  $[\text{Au}_{13}(\text{PPhMe}_2)_{10}\text{Cl}_2]\text{[PF}_6^-$ ]<sub>3</sub>, the only other crystallographically characterized monophosphine-protected icosahedral Au<sub>13</sub> cluster (see also Table S3†).<sup>4</sup>

Consistent with the formulation, the ESI-MS(+) spectra of **2a**·Cl and **2a**·PF<sub>6</sub> both show a main peak at  $m/z \sim 2746$  with an isotopic interval of 0.5 amu, indicating a +2 charge (Fig. 4 and S31†). This is thus attributable to the fragment ion  $[M-Cl]^{2+}$ , *i.e.*,  $[Au_{13}(SbPh_3)_8Cl_3]^{2+}$ ; the experimental isotopic pattern matches well with the calculated pattern. Similarly, the mass spectrum for **2b**·Cl shows a major ion fragment at  $m/z \sim 2914$  assignable to the  $[M-Cl]^{2+}$  ion (Fig. S32†).

While a solid sample of **2a**·Cl kept at 4 °C without exclusion of air remained intact after ten months, as manifested by the  $^1\text{H}$  NMR spectrum (Fig. S22†), a solution in DCM or acetone showed the formation of a small amount of an unidentified product after several days under ambient conditions. Decomposition in acetone was almost complete after four months; the mass spectrum of the resulting brown mixture suggests the presence of  $\text{Ph}_3\text{SbClX}$  (X = Cl or OH), indicating dissociation and oxidation of the ligands (Fig. S33†). The decomposition process also appears to be solvent dependent although the nature of this is unclear (Fig. S23 and S24†). The *p*-tolyl

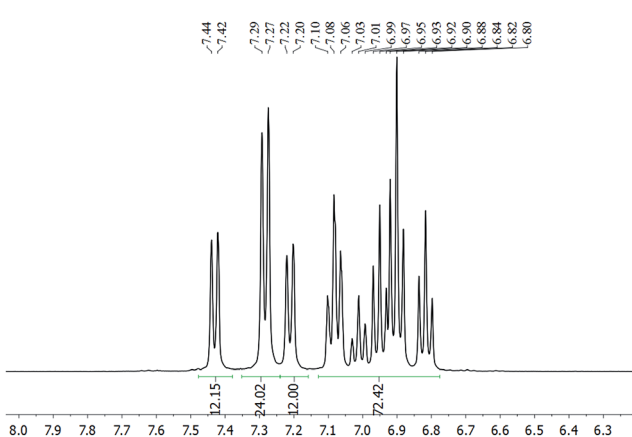


Fig. 2  $^1\text{H}$  NMR spectrum of **2a** $\cdot\text{PF}_6$  in  $\text{CD}_2\text{Cl}_2$  (aromatic region).

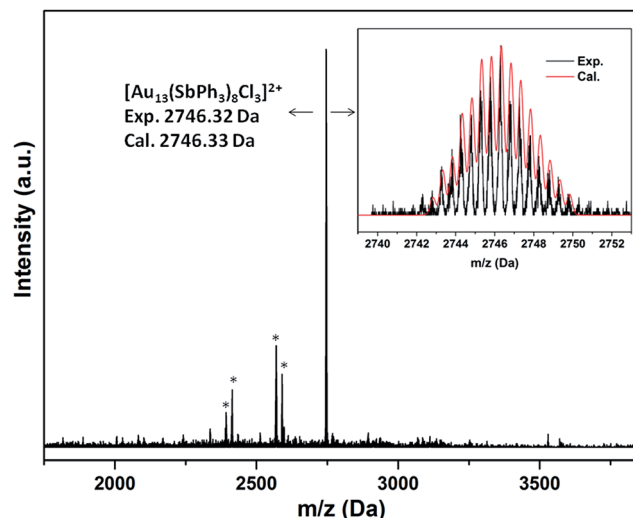


Fig. 4 ESI-MS(+) spectrum of  $2\mathbf{a}\cdot\text{PF}_6$ . The asterisks indicate fragments corresponding to loss of  $\text{SbPh}_3$  ligands. Inset: calculated and experimental patterns of the main ion fragment.

analogue  $2\mathbf{b}\cdot\text{Cl}$  displayed similar stability in solution (Fig. S25†). These stibine-protected  $\text{Au}_{13}$  clusters are stable to natural light but somewhat sensitive to UV light (254 nm) in solution. The lower thermal stability of  $2\cdot\text{Cl}$  compared to phosphine-protected  $\text{Au}_{11}$  clusters such as  $[\text{Au}_{11}(\text{PPh}_3)_8\text{Cl}_2][\text{Cl}]$  may be ascribable to the lower coordinating ability of the stibine ligands. Consistent with this is the observation that treatment of  $2\mathbf{b}\cdot\text{Cl}$  with excess  $\text{PPh}_3$  led readily to the formation of  $[\text{Au}_{11}(\text{PPh}_3)_8\text{Cl}_2][\text{Cl}]$  (Fig. S29 and S40†). TGA and DTG measurements on  $2\mathbf{a}\cdot\text{PF}_6$  and  $[\text{Au}_{11}(\text{PPh}_3)_8\text{Cl}_2][\text{Cl}]$  also clearly demonstrate that the former possesses lower thermal stability; decomposition corresponding to loss of all ligands occurred at  $\sim 155$  °C and  $\sim 172$  °C, respectively (Fig. S7†).

### Optical and electrochemical properties

The electronic spectra of  $2\mathbf{a}\cdot\text{X}$  ( $\text{X} = \text{Cl}, \text{PF}_6, \text{BPh}_4$ ) and  $2\mathbf{b}\cdot\text{Cl}$ , are essentially identical (Fig. 5), pointing to a common ( $\text{Au}_{13}$ ) metal core. There are two main absorption peaks at 352 and 454 nm, together with several weaker absorptions around 490, 530, 580 and 620 nm. The two main peaks are red-shifted compared to the 340 and 430 nm reported for the phosphine-protected clusters  $[\text{Au}_{13}(\text{L})_4\text{Cl}_4][\text{Cl}]$  ( $\text{L}$  = diphosphine) and  $[\text{Au}_{13}(\text{L})_8\text{Cl}_4][\text{Cl}]$  ( $\text{L}$  = monophosphine), all of which contain a closed icosahedral  $\text{Au}_{13}$  core.<sup>14b,16</sup> The UV-Vis spectra also appear to be solvent-independent; the main absorption peak of  $2\mathbf{b}\cdot\text{Cl}$  in acetonitrile is slightly blue-shifted compared to that in DCM or ethanol (Fig. S41†). A time-dependant DFT (TDDFT) calculation performed on the cationic fragment  $[\text{Au}_{13}(\text{SbPh}_3)_8\text{Cl}_4]^+$ ,  $2\mathbf{a}$ , at the MPW1PW91/LANL2DZ level of theory shows two strong peaks in the calculated spectrum at *ca.* 338 nm and 436 nm, which may correspond to the observed peaks at 352 nm and 454 nm (Fig. 5). Both peaks are due to several transitions; the transitions for the former are primarily LMCT in nature, and those for the latter are mainly metal-to-metal transitions (Table S2 and Fig. S8†). The red shift with respect to the

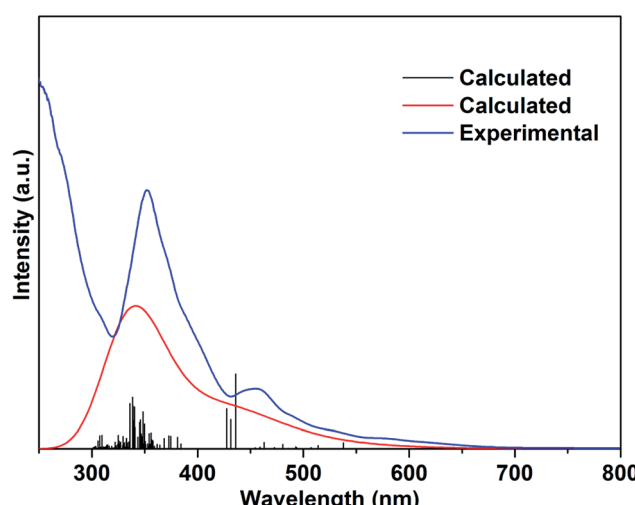
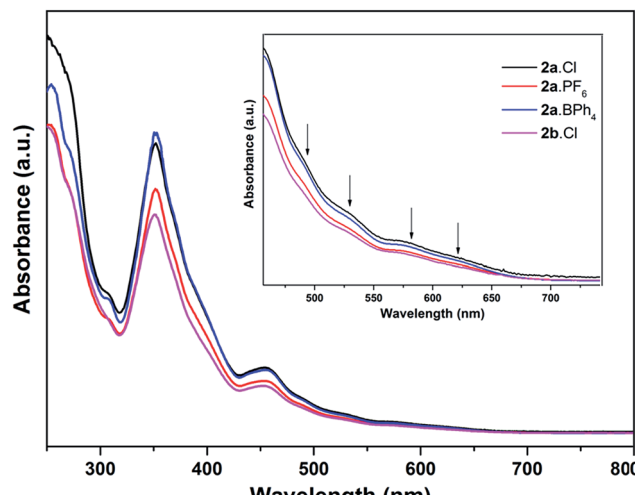


Fig. 5 Top: electronic spectra of  $2\mathbf{a}\cdot\text{X}$  ( $\text{X} = \text{Cl}, \text{PF}_6, \text{BPh}_4$ ) and  $2\mathbf{b}\cdot\text{Cl}$  in dichloromethane. Inset: the enlarged spectra for the lower-energy adsorption peaks. Bottom: comparison of the calculated (TDDFT) and experimental UV-Vis electronic spectra of  $2\mathbf{a}$ .

phosphine-protected clusters can thus be understood in terms of the difference in the Au-L interactions and is believed to be related to the weaker  $\sigma$ -basicity and stronger  $\pi$ -acidity of the stibines compared to phosphines.<sup>25</sup> Such a “heavier ligand displacement” effect has previously been observed in thiolate-protected clusters.<sup>26</sup>

Thiolate-protected gold nanoclusters display weak photoluminescence in the visible to near-infrared (NIR) region with a low quantum yield (<0.1%),<sup>27</sup> although some with specific core-shell structures,<sup>28</sup> or specific ligands such as peptides,<sup>29</sup> have been reported to show stronger emissions, demonstrating the importance of the protecting ligands in tuning the luminescence.<sup>30</sup> An example is that of  $[\text{Au}_{25}(\text{SC}_2\text{H}_4\text{Ph})_{18}][\text{TOA}]$  and  $[\text{Au}_{25}(\text{SePh})_{18}][\text{TOA}]$ , with the latter displaying a 25 nm red-shifted luminescence compared to the former.<sup>26b</sup> Similarly, the diphosphine-protected clusters  $[\text{Au}_{13}(\text{dppe})_5(\text{X})_2]^{3+}$  ( $\text{X} = \text{Cl}; \text{CCPh}$ ) have been reported to show an emission maximum at *ca.* 800 nm, while that in  $[\text{Au}_{13}(\text{dppp})_4(\text{Cl})_4][\text{Cl}]$  and  $[\text{Au}_{13}(\text{TOP})_8\text{Cl}_4][\text{Cl}]$  are blue-shifted to *ca.* 775 nm.<sup>14b</sup> In comparison, the

stibine-protected  $\text{Au}_{13}$  clusters  $2\mathbf{a}\cdot\text{X}$  ( $\text{X} = \text{Cl}, \text{PF}_6, \text{BPh}_4$ ) and  $2\mathbf{b}\cdot\text{Cl}$  show an NIR emission at *ca.* 740 nm, along with a shoulder at *ca.* 825 nm, *i.e.*, a further blue shift of *ca.* 35 nm (Fig. 6). Thus a more electron-donating ligand leads to lower energy transitions and emissions. In addition, it is noted that  $2\mathbf{a}\cdot\text{Cl}$  and  $2\mathbf{b}\cdot\text{Cl}$  show weaker luminescence intensities than  $2\mathbf{a}\cdot\text{PF}_6$  and  $2\mathbf{a}\cdot\text{BPh}_4$ , indicating that the counterion  $\text{Cl}^-$  may have a quenching effect.

The cyclic voltammogram (CV) of  $2\mathbf{a}\cdot\text{PF}_6$  in DCM with  ${}^n\text{Bu}_4\text{NPF}_6$  as the supporting electrolyte shows that the cluster undergoes irreversible oxidation and reduction (Fig. 7). While electron transfers occurring between  $-2.5$  and  $+1.0$  V are reproducible, *i.e.*, the redox peaks in both the positive and negative potential directions overlap, those occurring beyond  $+1.0$  V are not, presumably arising from breakdown of the cluster compound (Fig. S36†). The redox behavior of  $2\mathbf{a}\cdot\text{PF}_6$  between  $-2.5$  and  $+1.0$  V is therefore reliable for analysis of its electrochemical properties. In this region, three oxidation peaks were found at  $+0.34, +0.58$  and  $+0.78$  V in the square-wave voltammogram (SWV), probably corresponding to oxidation to the  $+2, +3$  and  $+4$  states, respectively; seven reduction peaks ( $-1.51, -1.61, -1.68, -1.77, -1.97, -2.11, -2.22$  V) were observed in the same region. The electrochemical HOMO–LUMO energy gap was determined to be about 1.85 eV (without subtracting the charge energy) from the first oxidation and reduction potentials ( $\text{O}1$  and  $\text{R}1$ ), which is in excellent agreement with that derived from the UV-Vis spectral data (620 nm absorption peak) by extrapolation to zero absorbance. In comparison, the other two  $\text{Au}_{13}$  clusters [ $\text{Au}_{13}(\text{PPh}_3)_4(\text{SC}_{12}\text{H}_{25})_2\text{Cl}_2$ ] and [ $\text{Au}_{13}(\text{dppm})_6\text{Cl}_5$ ], with closed and open icosahedral metal core geometries, have lower HOMO–LUMO gaps of 1.76 and 1.66 eV, respectively.<sup>13,31</sup>

### Conversion to $\text{Au}_{25}$ cluster

Water-soluble, peptide-protected  $\text{Au}_{25}$  clusters possessing relatively strong fluorescence, such as  $[\text{Au}_{25}(\text{SG})_{18}]$ , **4**, have wide

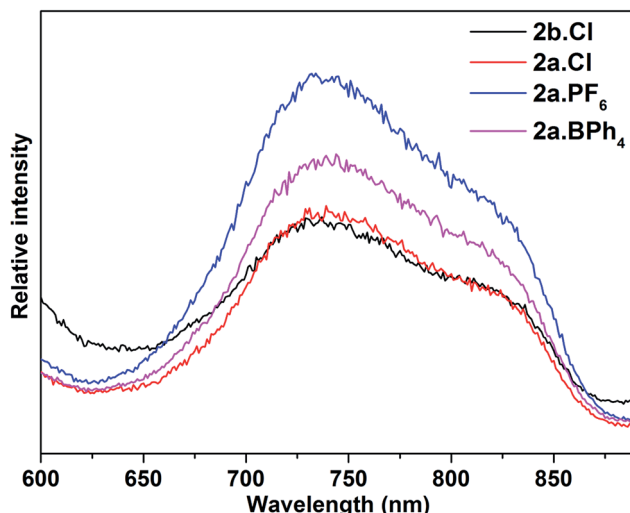


Fig. 6 Photoluminescence spectra of  $2\mathbf{a}\cdot\text{X}$  ( $\text{X} = \text{Cl}, \text{PF}_6, \text{BPh}_4$ ) and  $2\mathbf{b}\cdot\text{Cl}$  ( $\lambda_{\text{ex}} = 470$  nm) in DCM solution at room temperature (concentration: *ca.* 1.0 mg ml<sup>-1</sup>).

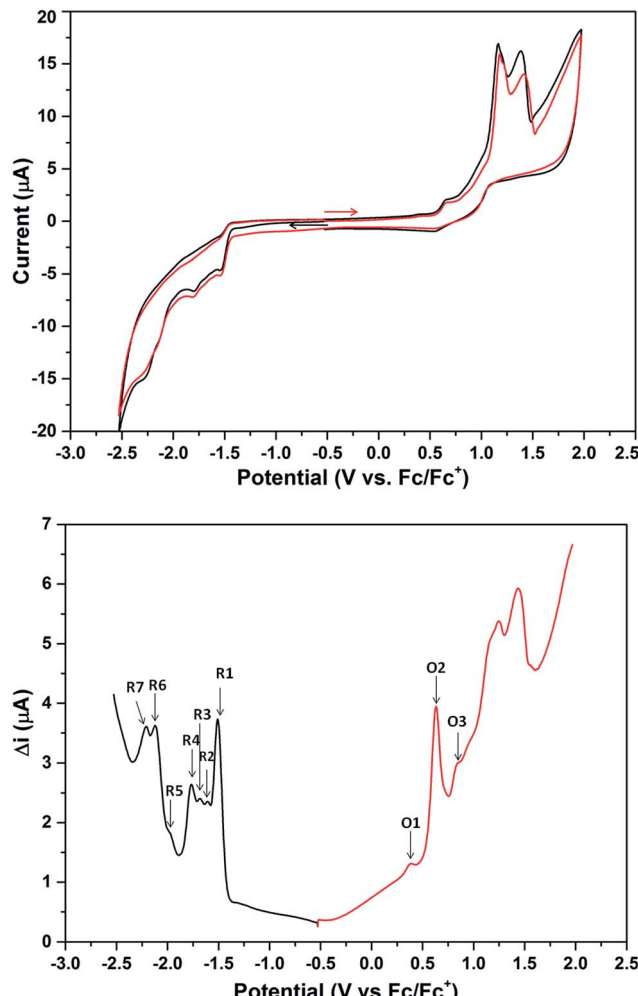
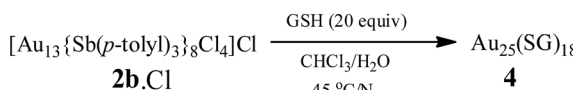


Fig. 7 CV (top) and DSV (bottom) spectra of  $2\mathbf{a}\cdot\text{PF}_6$  in DCM (1.0 mM) with 0.10 M  ${}^n\text{Bu}_4\text{NPF}_6$  as the supporting electrolyte. Working electrode: 1 mm diameter planar glassy carbon; auxiliary electrode: Pt wire; pseudo-reference electrode: Ag wire (in 0.50 M  ${}^n\text{Bu}_4\text{NPF}_6$  in  $\text{CH}_3\text{CN}$ ); scan rate: 0.10 V s<sup>-1</sup>; ferrocene (Fc) was added as an internal reference at the end of the experiment. For CV, the scans were initiated in the positive (red) and negative (black) potential directions, respectively. For SWV, the red and blue traces were scanned in the positive and negative potential directions, respectively. Pulse period ( $\tau$ ) = 25 Hz; potential step = 5.0 mV; pulse amplitude = 20 mV.

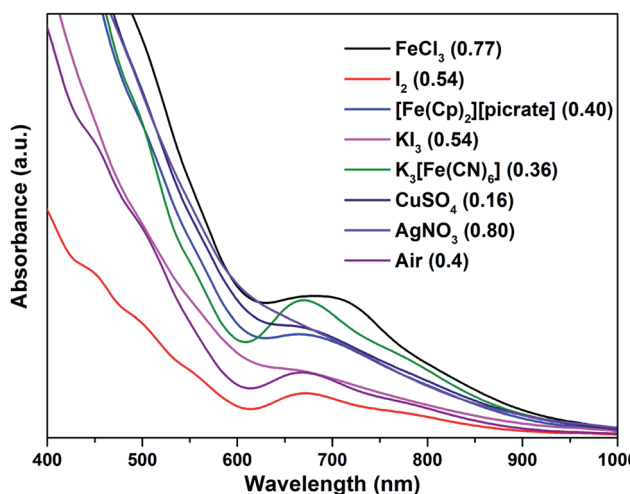
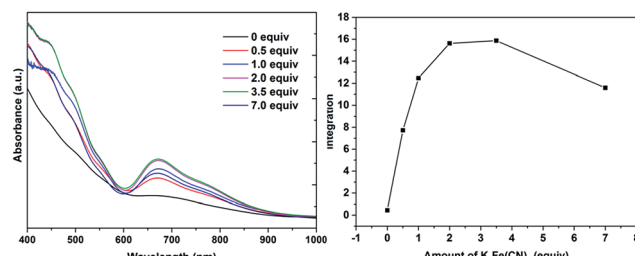
applications in sensing, imaging and biomedicine.<sup>32</sup> Although they can be prepared by the modified Brust method, *viz.*, reduction of the putative  $[\text{Au}(\text{i}-\text{SR})_n]$  oligomer with suitable reducing agents,<sup>33</sup> it has been found recently that treatment of  $\text{PPh}_3$ -protected  $\text{Au}_{11}$  nanoclusters or larger nanoparticles,<sup>15,34</sup> or thiolate-protected colloidal clusters  $[\text{Au}_n(\text{SG})_m]$ ,<sup>35</sup> with excessive glutathione (GSH) is a more efficient synthetic route to **4**. Although the exact mechanism for the ligand exchange is unclear,<sup>36</sup> it is strongly associated with the stability of the reactant clusters, as indicated by the observation that while  $[\text{Au}_{11}(\text{PPh}_3)_7\text{Cl}_3]$  undergoes ligand exchange with GSH to give **4**, the more structurally stable ionic clusters  $[\text{Au}_{11}(\text{PPh}_3)_8\text{Cl}_2]\text{Cl}$  and  $[\text{Au}_{11}(\text{dppf})_4\text{Cl}_2]\text{Cl}$  do not react with GSH under the same conditions.<sup>15,4d</sup> Given the weaker coordinating ability of stibines compared to phosphines, the ligand exchange reaction between



Scheme 2 Ligand exchange reaction of **2b.Cl** with GSH.

2 and thiolates may be expected to occur more readily. Indeed, ligand exchange in **2b.Cl** with GSH does occur, and the formation of **4** can be monitored by its characteristic peak at  $\sim 670$  nm (Scheme 2). In comparison, unlike the case with  $\text{PPh}_3$ , the reaction of  $[\text{Au}_{25}(\text{SC}_2\text{H}_4\text{Ph})_{18}][\text{TOA}]$  with  $\text{Sb}(p\text{-tolyl})_3$  (20 and 60 equiv.) did not appear to give any of a biicosahedral rod  $[\text{Au}_{25}\{\text{Sb}(p\text{-tolyl})_3\}_{10}(\text{SR})_5\text{Cl}_2]^{2+}$ .<sup>37</sup>

The formation of **4** was detectable after 4 h (Fig. S42†). In comparison,  $[\text{Au}_{11}(\text{PPh}_3)_7\text{Cl}_3]$  was reported to show the formation of **4** after more than 6 h at  $50^\circ\text{C}$ , while the cationic  $[\text{Au}_{11}(\text{PPh}_3)_8\text{Cl}_2][\text{Cl}]$  showed even lower reactivity although air was found to aid the reaction.<sup>34a</sup> The important role of air was also apparent for **2b.Cl**; under aerobic conditions, the formation of **4** was apparent from about 90 min (Fig. S43†), with a higher reaction rate than under anaerobic conditions (Fig. S44 and S45†). Since the fraction of  $\text{Au}(\text{i})$  to  $\text{Au}$  atoms changed from 0.38 to 0.72 in the conversion of **2b** to **4**, we hypothesize that the oxygen in air acts as an oxidant to facilitate the conversion; such an oxidation-induced transformation of smaller clusters to larger clusters has received much attention recently.<sup>38</sup> To test the idea that oxidation is involved, the conversion was carried out with a variety of oxidants (0.50 equiv.) with differing oxidation potential and solubility. The addition of an oxidant clearly affected the rate of conversion, although we could not find any clear correlation between the conversion rate and the oxidation potential or solubility of the oxidant (Fig. 8 and S46–S53†). Besides air, the oxidants  $\text{K}_3[\text{Fe}(\text{CN})_6]$  and  $\text{I}_2$  showed significant acceleration of the conversion while others showed only moderate to poor effects. The addition of more  $\text{K}_3[\text{Fe}(\text{CN})_6]$  from 0.5 equiv.

Fig. 8 Electronic spectra of the aqueous solution for the conversion of **2b.Cl** to **4** with different oxidants, at 240 min reaction time. Redox potential (V) vs. SHE for oxidants given in parenthesis.<sup>39</sup>Fig. 9 Electronic spectra of the aqueous solution for the conversion of **2b.Cl** to **4** with varying amount of  $\text{K}_3[\text{Fe}(\text{CN})_6]$ , at 240 min reaction time (left), and the characteristic peak integration vs. amount of  $\text{K}_3[\text{Fe}(\text{CN})_6]$  (right).

to 3.5 equiv. (the theoretical amount required to change the fraction of  $\text{Au}(\text{i})$  to  $\text{Au}(0)$  atoms in **2b.Cl** from 0.38 to 0.72) increased the conversion rate further but further addition to 7.0 equiv. led to a decrease in the conversion rate (Fig. 9 and S54–S57†).

Although antagalvanic reduction is a possibility,<sup>40</sup> the mechanism for the conversion is not entirely clear. In the conversion mediated by  $\text{K}_3[\text{Fe}(\text{CN})_6]$ , a small amount of Prussian blue was formed, identified by comparison of its IR spectral characteristics with that of an authentic sample (Fig. S58†). This is presumably formed from the reduced  $[\text{Fe}(\text{CN})_6]^{4-}$  and hydrolysed forms of the more labile  $[\text{Fe}(\text{CN})_6]^{3-}$ . Although the stibine and GSH were found to be able to reduce  $\text{K}_3[\text{Fe}(\text{CN})_6]$  to  $\text{K}_4[\text{Fe}(\text{CN})_6]$  under the same reaction conditions, no Prussian blue formation was observed (Fig. S58†), indirectly pointing to involvement of the  $\text{Au}$  core rather than the ligand sphere of **2b.Cl**. An inner sphere electron transfer, presumably involving bridging CN-ligands, may therefore be operative. Consistent with this was that treatment of **2b.Cl** with  $\text{K}_3[\text{Fe}(\text{CN})_6]$  (3.5 equiv) indeed led to decomposition of **2b.Cl** and the formation of Prussian blue (Fig. S58†).

## Conclusion

We have reported here, for the first time,  $\text{Au}$  nanoclusters with stibines as protecting ligands. In contrast to phosphines, the use of stibines as the protecting ligand favors the formation of icosahedral  $\text{Au}_{13}$  clusters rather than  $\text{Au}_{11}$  or a polydispersed mixture of smaller clusters and they made for interesting comparison with, and a better understanding of, the structures of the phosphine analogues. The weaker coordinating ability of the stibine ligands also made them promising precursors to other  $\text{Au}$  nanoclusters, for example, to the thiolate protected  $\text{Au}_{25}$  cluster. More importantly, we have found that the addition of a suitable oxidant can significantly increase the conversion rate by aiding the size-focusing process.

## Conflicts of interest

There are no conflicts to declare.



## Acknowledgements

This work was supported by a research grant (SERC grant no. 1521200076) from the Agency for Science, Technology and Research (A\*STAR), Singapore.

## Notes and references

- (a) P. D. Jazdinsky, G. Calero, C. J. Ackerson, D. A. Bushnell and R. D. Kornberg, *Science*, 2007, **318**, 430–433; (b) M. Zhu, C. M. Aikens, F. J. Hollander, G. C. Schatz and R. Jin, *J. Am. Chem. Soc.*, 2008, **130**, 5883–5885; (c) M. W. Heaven, A. Dass, P. S. White, K. M. Holt and R. W. Murray, *J. Am. Chem. Soc.*, 2008, **130**, 3754–3755; (d) H. Qian, W. T. Eckenhoff, Y. Zhu, T. Pintauer and R. Jin, *J. Am. Chem. Soc.*, 2010, **132**, 8280–8281; (e) I. Dolamic, S. Knoppe, A. Dass and T. Bürgi, *Nat. Commun.*, 2012, **3**, 798; (f) C. Liu, T. Li, G. Li, K. Nobusada, C. Zeng, G. Pang, N. L. Rosi and R. Jin, *Angew. Chem., Int. Ed.*, 2015, **54**, 9826–9829; (g) R. C. Jin, *Nanoscale*, 2015, **7**, 1549–1565; (h) D. Crasto, G. Barcaro, M. Stener, L. Sementa, A. Fortunelli and A. Dass, *J. Am. Chem. Soc.*, 2014, **136**, 14933–14940; (i) D. Crasto, S. Malola, G. Brosofsky, A. Dass and H. Häkkinen, *J. Am. Chem. Soc.*, 2014, **136**, 5000–5005; (j) S. Chen, S. Wang, J. Zhong, Y. Song, J. Zhang, H. Sheng, Y. Pei and M. Zhu, *Angew. Chem., Int. Ed.*, 2015, **54**, 3145–3149; (k) C. J. Zeng, Y. X. Chen, K. Kirschbaum, K. J. Lambright and R. C. Jin, *Science*, 2016, **354**, 1580–1584; (l) R. Jin, C. Zeng, M. Zhou and Y. Chen, *Chem. Rev.*, 2016, **116**, 10346–10413; (m) K. M. O. Jensen, P. Juhas, M. A. Tofanelli, C. L. Heinecke, G. Vaughan, C. J. Ackerson and S. J. L. Billinge, *Nat. Commun.*, 2016, **7**, 11859; (n) W. Kurashige, Y. Niihori, S. Sharma and Y. Negishi, *Coord. Chem. Rev.*, 2016, **320–321**, 238–250.
- (a) X.-K. Wan, Q. Tang, S.-F. Yuan, D.-e. Jiang and Q.-M. Wang, *J. Am. Chem. Soc.*, 2015, **137**, 652–655; (b) X. K. Wan, S. F. Yuan, Q. Tang, D.-E. Jiang and Q. M. Wang, *Angew. Chem., Int. Ed.*, 2015, **54**, 5977–5980; (c) X. K. Wan, W. W. Xu, S. F. Yuan, Y. Gao, X. C. Zeng and Q. M. Wang, *Angew. Chem., Int. Ed.*, 2015, **54**, 9683–9686; (d) Z. Lei, X.-K. Wan, S.-F. Yuan, J.-Q. Wang and Q.-M. Wang, *Dalton Trans.*, 2017, **46**, 3427–3434; (e) X.-K. Wan, Z.-J. Guan and Q.-M. Wang, *Angew. Chem., Int. Ed.*, 2017, **56**, 11494–11497.
- L. Naldini, F. Cariati, G. Simonetta and L. Malatesta, *Chem. Commun.*, 1966, 647–648.
- (a) J. W. A. Van der Velden, P. T. Beurskens, J. J. Bour, W. P. Bosman, J. H. Noordik, M. Kolenbrander and J. A. K. M. Buskes, *Inorg. Chem.*, 1984, **23**, 146–151; (b) J. W. A. Van der Velden, J. J. Bour, W. P. Bosman and J. H. Noordik, *Inorg. Chem.*, 1983, **22**, 1913–1918; (c) F. Wen, U. Englert, B. Gutrat and U. Simon, *Eur. J. Inorg. Chem.*, 2008, **2008**, 106–111; (d) L.-Y. Yao and V. W.-W. Yam, *J. Am. Chem. Soc.*, 2016, **138**, 15736–15742; (e) D. P. Anderson, J. F. Alvino, A. Gentleman, H. A. Qahtani, L. Thomsen, M. I. Polson, G. F. Metha, V. B. Golovko and G. G. Andersson, *Phys. Chem. Chem. Phys.*, 2013, **15**, 3917–3929; (f) C. E. Briant, B. R. C. Theobald, J. W. White, L. K. Bell, D. M. P. Mingos and A. J. Welch, *J. Chem. Soc., Chem. Commun.*, 1981, 201–202; (g) X.-K. Wan, S.-F. Yuan, Z.-W. Lin and Q.-M. Wang, *Angew. Chem., Int. Ed.*, 2014, **53**, 2923–2926; (h) J. Chen, Q.-F. Zhang, P. G. Williard and L.-S. Wang, *Inorg. Chem.*, 2014, **53**, 3932–3934; (i) B. K. Teo, X. Shi and H. Zhang, *J. Am. Chem. Soc.*, 1992, **114**, 2743–2745.
- (a) B. S. Gutrat, U. Englert, Y. Wang and U. Simon, *Eur. J. Inorg. Chem.*, 2013, **2013**, 2002–2006; (b) B. S. Gutrat, I. M. Oppel, O. Presly, I. Beljakov, V. Meded, W. Wenzel and U. Simon, *Angew. Chem., Int. Ed.*, 2013, **52**, 3529–3532; (c) J. Chen, Q.-F. Zhang, T. A. Bonaccorso, P. G. Williard and L.-S. Wang, *J. Am. Chem. Soc.*, 2014, **136**, 92–95; (d) Q.-F. Zhang, P. G. Williard and L.-S. Wang, *Small*, 2016, **12**, 2518–2525.
- G. Schmid, R. Pfeil, R. Boese, F. Bandermann, S. Meyer, G. H. M. Calis and J. W. A. van der Velden, *Chem. Ber.*, 1981, **114**, 3634–3642.
- W. W. Weare, S. M. Reed, M. G. Warner and J. E. Hutchison, *J. Am. Chem. Soc.*, 2000, **122**, 12890–12891.
- (a) Y. Shichibu, Y. Negishi, T. Watanabe, N. K. Chaki, H. Kawaguchi and T. Tsukuda, *J. Phys. Chem. C*, 2007, **111**, 7845–7847; (b) J.-i. Nishigaki, S. Yamazoe, S. Kohara, A. Fujiwara, W. Kurashige, Y. Negishi and T. Tsukuda, *Chem. Commun.*, 2014, **50**, 839–841; (c) R. Jin, C. Liu, S. Zhao, A. Das, H. Xing, C. Gayathri, Y. Xing, N. L. Rosi, R. R. Gil and R. Jin, *ACS Nano*, 2015, **9**, 8530–8536; (d) Y. Song, F. Fu, J. Zhang, J. Chai, X. Kang, P. Li, S. Li, H. Zhou and M. Zhu, *Angew. Chem., Int. Ed.*, 2015, **54**, 8430–8434.
- (a) H. Yang, Y. Wang, J. Lei, L. Shi, X. Wu, V. Makinen, S. Lin, Z. Tang, J. He, H. Hakkinen, L. Zheng and N. Zheng, *J. Am. Chem. Soc.*, 2013, **135**, 9568–9571; (b) H. Yang, Y. Wang, J. Yan, X. Chen, X. Zhang, H. Häkkinen and N. Zheng, *J. Am. Chem. Soc.*, 2014, **136**, 7197–7200.
- B. Fresch, E. Hanozin, F. Dufour and F. Remacle, *Eur. Phys. J. D*, 2012, **66**, 326–335.
- J. W. A. van der Velden, F. A. Vollenbroek, J. J. Bour, P. T. Beurskens, J. M. M. Smits and W. P. Bosnian, *Recl. Trav. Chim. Pays-Bas*, 1981, **100**, 148–152.
- S. Jin, W. Du, S. Wang, X. Kang, M. Chen, D. Hu, S. Chen, X. Zou, G. Sun and M. Zhu, *Inorg. Chem.*, 2017, **56**, 11151–11159.
- S.-S. Zhang, L. Feng, R. D. Senanayake, C. M. Aikens, X.-P. Wang, Q.-Q. Zhao, C.-H. Tung and D. Sun, *Chem. Sci.*, 2018, **9**, 1251–1258.
- (a) Y. Shichibu and K. Konishi, *Small*, 2010, **6**, 1216–1220; (b) Y. Shichibu, K. Suzuki and K. Konishi, *Nanoscale*, 2012, **4**, 4125–4129; (c) M. Sugiuchi, Y. Shichibu, T. Nakanishi, Y. Hasegawa and K. Konishi, *Chem. Commun.*, 2015, **51**, 13519–13522.
- L. C. McKenzie, T. O. Zaikova and J. E. Hutchison, *J. Am. Chem. Soc.*, 2014, **136**, 13426–13435.
- R. C. B. Copley and D. M. P. Mingos, *J. Chem. Soc., Dalton Trans.*, 1996, 491–500.



17 (a) P. D. Cookson and E. R. T. Tiekkink, *Acta Crystallogr., Sect. C: Struct. Chem.*, 1994, **50**, 1896–1898; (b) R. C. Bott, P. C. Healy and G. Smith, *Aust. J. Chem.*, 2004, **57**, 213–218.

18 H. Schmidbaur and A. Schier, *Chem. Soc. Rev.*, 2012, **41**, 370–412.

19 Crystallographically, the anion in **3a** was modelled as disordered between a  $[\text{Ph}_2\text{SbCl}_2]^-$  and a chloride; with appropriate restraints, the final occupancies were ~93% and 7%, respectively. See Fig. S4† for the Ortep diagram.

20 T. Huang, L. Huang, Y. Jiang, F. Hu, Z. Sun, G. Pan and S. Wei, *Dalton Trans.*, 2017, **46**, 12239–12244.

21 E. B. Guidez, A. Hadley and C. M. Aikens, *J. Phys. Chem. C*, 2011, **115**, 6305–6316.

22 L. Falivene, R. Credendino, A. Poater, A. Petta, L. Serra, R. Oliva, V. Scarano and L. Cavallo, *Organometallics*, 2016, **35**, 2286–2293. See the ESI (Fig. S59†) for more details.

23 (a) B. M. Barnsgrover and C. M. Aikens, *J. Phys. Chem. Lett.*, 2011, **2**, 990–994; (b) Z. Luo, V. Nachammai, B. Zhang, N. Yan, D. T. Leong, D. E. Jiang and J. Xie, *J. Am. Chem. Soc.*, 2014, **136**, 10577–10580.

24 (a) M. Walter, J. Akola, O. Lopez-Acevedo, P. D. Jazdzinsky, G. Calero, C. J. Ackerson, R. L. Whetten, H. Grönbeck and H. Häkkinen, *Proc. Natl. Acad. Sci.*, 2008, **105**, 9157–9162; (b) D. E. Jiang, M. Kuhn, Q. Tang and F. Weigend, *J. Phys. Chem. Lett.*, 2014, **5**, 3286–3289; (c) D. E. Jiang and S. Dai, *Inorg. Chem.*, 2009, **48**, 2720–2722.

25 S. L. Benjamin and G. Reid, *Coord. Chem. Rev.*, 2015, **297**, 168–180.

26 (a) X. Meng, Q. Xu, S. Wang and M. Zhu, *Nanoscale*, 2012, **4**, 4161–4165; (b) Y. Song, J. Zhong, S. Yang, S. Wang, T. Cao, J. Zhang, P. Li, D. Hu, Y. Pei and M. Zhu, *Nanoscale*, 2014, **6**, 13977–13985.

27 (a) S. Link, A. Beeby, S. FitzGerald, M. A. El-Sayed, T. G. Schaaff and R. L. Whetten, *J. Phys. Chem. B*, 2002, **106**, 3410; (b) T. Huang and R. W. Murray, *J. Phys. Chem. B*, 2001, **105**, 12498; (c) Y. Negishi, K. Nobusada and T. Tsukuda, *J. Am. Chem. Soc.*, 2005, **127**, 5261; (d) F. Aldeek, M. A. H. Muhammed, G. Palui, N. Zhan and H. Matoussi, *ACS Nano*, 2013, **7**, 2509.

28 Z. Gan, Y. Lin, L. Luo, G. Han, W. Liu, Z. Liu, C. Yao, L. Weng, L. Liao, J. Chen, X. Liu, Y. Luo, C. Wang, S. Wei and Z. Wu, *Angew. Chem., Int. Ed.*, 2016, **55**, 11567–11571.

29 (a) Y. Yu, S. Y. New, J. Xie, X. Su and Y. N. Tan, *Chem. Commun.*, 2014, **50**, 13805; (b) Y. Yu, Z. Luo, D. M. Chevrier, D. T. Leong, P. Zhang, D. E. Jiang and J. Xie, *J. Am. Chem. Soc.*, 2014, **136**, 1246–1249.

30 Z. Wu and R. Jin, *Nano Lett.*, 2010, **10**, 2568.

31 L. D. Menard, S.-P. Gao, H. Xu, R. D. Twesten, A. S. Harper, Y. Song, G. Wang, A. D. Douglas, J. C. Yang, A. I. Frenkel, R. G. Nuzzo and R. W. Murray, *J. Phys. Chem. B*, 2006, **110**, 12874–12883.

32 (a) L.-Y. Chen, C.-W. Wang, Z. Yuan and H.-T. Chang, *Anal. Chem.*, 2015, **87**, 216–229; (b) Y. Zheng, L. Lai, W. Liu, H. Jiang and X. Wang, *Adv. Colloid Interface Sci.*, 2017, **242**, 1–16.

33 Z. Wu, J. Suhan and R. Jin, *J. Mater. Chem.*, 2009, **19**, 622–626.

34 (a) Y. Shichibu, Y. Negishi, T. Tsukuda and T. Teranishi, *J. Am. Chem. Soc.*, 2005, **127**, 13464–13465; (b) H. Qian, M. Zhu, E. Lanni, Y. Zhu, M. E. Bier and R. Jin, *J. Phys. Chem. C*, 2009, **113**, 17599–17603; (c) J. Lin, W. Li, C. Liu, P. Huang, M. Zhu, Q. Ge and G. Li, *Nanoscale*, 2015, **7**, 13663–13670.

35 S. Yukatsu, N. Yuichi, T. Hironori, K. Masayuki, T. Toshiharu and T. Tatsuya, *Small*, 2007, **3**, 835–839.

36 G. H. Woehrle, M. G. Warner and J. E. Hutchison, *J. Phys. Chem. B*, 2002, **106**, 9979–9981.

37 M.-B. Li, S.-K. Tian, Z. Wu and R. Jin, *Chem. Mater.*, 2016, **28**, 1022–1025.

38 (a) M.-B. Li, S.-K. Tian, Z. Wu and R. Jin, *Chem. Commun.*, 2015, **51**, 4433–4436; (b) T. Higaki, C. Liu, Y. Chen, S. Zhao, C. Zeng, R. Jin, S. Wang, N. L. Rosi and R. Jin, *J. Phys. Chem. Lett.*, 2017, **8**, 866–870; (c) X. Ren, J. Fu, X. Lin, X. Fu, J. Yan, R. a. Wu, C. Liu and J. Huang, *Dalton Trans.*, 2018, **47**, 7487–7491.

39 W. M. Haynes, *CRC handbook of chemistry and physics: a ready-reference book of chemical and physical data*, CRC Press, Boca Raton, Florida, 97th edn, 2016–2017, pp. 5–85.

40 Z. Wu, *Angew. Chem., Int. Ed.*, 2012, **51**, 2934–2938.